Catalysis Today xxx (2017) xxx–xxx

Contents lists available at ScienceDirect

Catalysis Today

journal homepage: www.elsevier.com/locate/cattod

In situ X-ray absorption spectroscopic studies of magnetic $Fe@Fe_xO_y/Pd$ nanoparticle catalysts for hydrogenation reactions

Yali Yao[a], Stefano Rubino[b], Byron D. Gates[b], Robert W.J. Scott[a,*], Yongfeng Hu[c,*]

[a] Department of Chemistry, 110 Science Place, University of Saskatchewan, Saskatoon, SK S7N 5C9, Canada
[b] Department of Chemistry and 4D LABS, Simon Fraser University, Burnaby, BC V5A 1S6, Canada
[c] Canadian Light Source, University of Saskatchewan, Saskatoon, SK S7N 2V3, Canada

ARTICLE INFO

Article history:
Received 4 July 2016
Received in revised form 28 January 2017
Accepted 27 February 2017
Available online xxx

Keywords:
$Fe@Fe_xO_y/Pd$ nanoparticles
in situ XANES study
Hydrogenation reactions
Solvent effect

ABSTRACT

Core@shell $Fe@Fe_xO_y$ nanoparticles (NPs) have attracted a great deal of interest as potential magnetic supports for catalytic metals *via* galvanic exchange reactions. In this study $Fe@Fe_xO_y/Pd$ bimetallic NPs were synthesized through galvanic exchange reactions using 50:1, 20:1 and 5:1 molar ratios of $Fe@Fe_xO_y$ NPs to $Pd(NO_3)_2$. The resulting $Fe@Fe_xO_y/Pd$ NPs have Pd NPs on the Fe oxide surfaces, and still retain their response to external magnetic fields. The materials could be recovered after the reaction by an external magnetic field, and agitation of the solution *via* a magnetic field led to improvements of mass transfer of the substrates to the catalyst surface for hydrogenation reactions. The $Fe@Fe_xO_y/Pd$ NPs derived from the 5:1 molar ratio of their respective salts (Fe:Pd) exhibited a higher catalytic activity than particles synthesized from 20:1 and 50:1 molar ratios for the hydrogenation of 2-methyl-3-buten-2-ol. The highest turnover frequency reached 3600 h^{-1} using ethanol as a solvent. *In situ* XANES spectra show that the $Fe@Fe_xO_y$ NPs in the $Fe@Fe_xO_y/Pd$ system are easily oxidized when dispersed in water, while they are very stable if ethanol is used as a solvent. This oxidative stability has important implications for the sustainable use of such particles in real world applications.

1. Introduction

Nanoparticles (NPs) can have dramatically different properties compared to their bulk counterparts due to their large surface-to-volume ratios and size-dependent electronic properties [1,2]. They have broad applications in catalysis, drug delivery, and environmental remediation [3–6]. Because of their small sizes, the separation of NPs from solutions after applications can be particularly problematic. Magnetic Fe or Fe oxide NPs have attracted tremendous attention, because they can be isolated from the liquid medium by simply applying an external magnetic field [7–9]. Moreover, Fe or Fe oxide NPs can respond to common magnetic stirrers, which opens up the possibilities of using them as nanoscale magnetic stir bars for mass transfer acceleration in microfluidic systems. For example, Chen's group assembled Fe_3O_4 NPs to form 1D chains preserved in a shell of silica [10]. The resulting Fe_3O_4 chains remain suspended and stir independently within a small liquid droplet. Song's group grafted Pd NPs on the surfaces of Fe_3O_4 nanochains using poly(cyclotriphosphazene-*co*-4,4′-sulfonyldiphenol) (PZS), and applied these nanochains as catalysts and nanometer-sized magnetic stir bars for microscopic hydrogenation reactions [11]. Considering that metallic Fe NPs also have interesting magnetic behavior, further studies into their magnetic performance and stability are required for applications in catalysis and microfluidic research.

Both Fe(0) and Fe(II) have relatively low standard electrode potentials (Fe^{2+}/Fe^0, $E^o_{1/2} = -0.447$ V, Fe^{3+}/Fe^{2+}, $E^o_{1/2} = 0.771$ V), so they can be used to reduce another metal onto their surfaces to form bimetallic NPs through galvanic exchange reactions [12]. Many bimetallic NPs, such as FePd, FeCu, FeRu, have been synthesized successfully by this method [13–16]. Recently, we showed that $Fe@Fe_xO_y$ NPs are very effective reductants for galvanic exchange reactions which can fully reduce Pd or Cu salts onto their surfaces to form Pd or Cu NPs [17]. We also demonstrated that these galvanic reactions can be monitored by *in situ* X-ray absorption spectroscopy (XAS). Depending on the metal deposited on the $Fe@Fe_xO_y$ NPs, the resulting bimetallic NPs can be used to further catalyze a variety of organic reactions. For example, Moores' group has shown that $Fe@Fe_xO_y@Cu$ NPs are active for the heterogeneous azide-alkyne click reactions and the cyclopropanation of diazoesters with styrene derivatives [14,18], and Zhou and

---

* Corresponding authors.
E-mail addresses: robert.scott@usask.ca (R.W.J. Scott), yongfeng.hu@lightsource.ca (Y. Hu).

http://dx.doi.org/10.1016/j.cattod.2017.02.049
0920-5861/

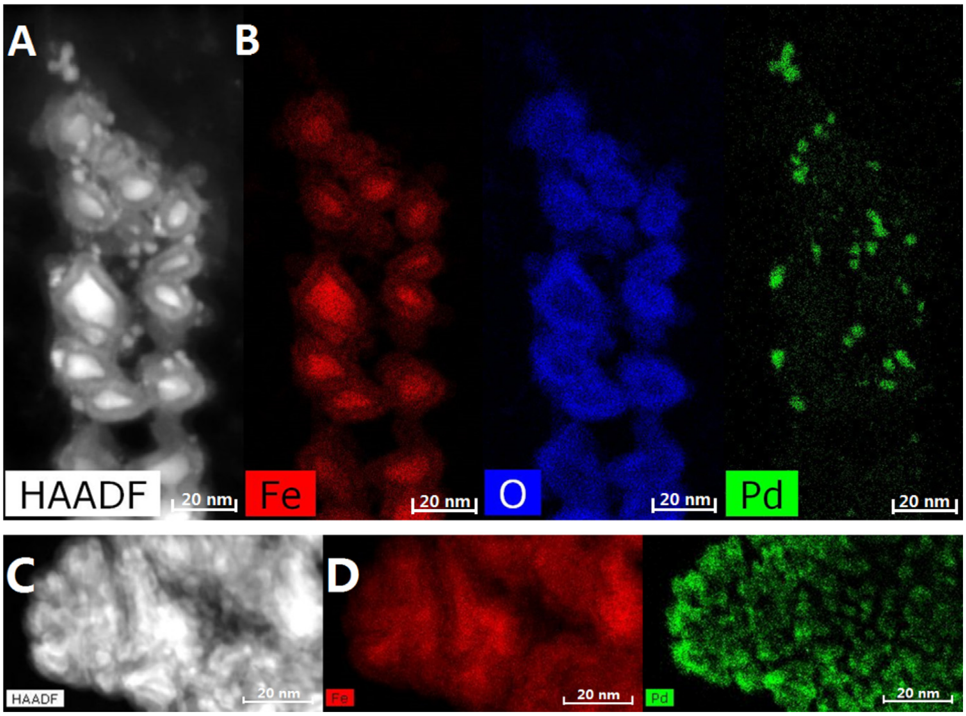

Fig. 1. High-angle annular dark-field STEM images and EDX elemental maps of the $Fe@Fe_xO_y/Pd$ NPs prepared from 20:1 (A and B) and 5:1 (C and D) molar ratios of $Fe@Fe_xO_y$ NPs to Pd (II).

coworkers have reported that $Fe@Fe_xO_y@Pd$ NPs are active catalysts for Suzuki-Miyaura cross-coupling reactions [13]. Pd can catalyze not only C—C coupling reactions, but also a myriad of hydrogenation reactions, and Pd/C is widely used as a catalyst for hydrogenation reactions [19–21]. A variety of supports have also been investigated to further improve the catalytic activity, stability and selectivity of Pd sites in different hydrogenation reactions. He and coworkers reported that covalent trizaine (CTF) framework-supported Pd NPs exhibit *ca.* 3.6 times faster reaction rates than Pd/C for the catalytic hydrogenation of N-methylpyrrole; the accelerated rate was attributed to intensified electronic interactions between the Pd NPs and the CTF [22]. The Fe_3O_4-PZS-Pd nanochains show much better stability during cycling tests for the hydrogenation of styrene in comparison with commercial Pd/C, because the interaction between PZS and Pd can efficiently prevent the aggregation of Pd NPs and the magnetic Fe_3O_4 component can assist with recovering these nanomaterials with almost no loss [11]. Studies of Fe-supported Pd NPs for catalytic hydrogenations are rare [23]. For many applications of the bimetallic NPs based on Fe as mentioned above, it is of great interest to investigate the performance of $Fe@Fe_xO_y@Pd$ NPs for hydrogenation reactions.

The study of the nature of a catalyst and the identity of its active site is important to improve its performance in catalytic reactions. *In situ* and *operando* characterizations of catalysts have been widely practiced by researchers, because they can directly probe catalysts under working conditions. Among various *in situ* techniques, X-ray absorption near edge structure (XANES) spectra are sensitive to the oxidation state and coordination environment of an element and can be used to probe short-range order within materials, and thus it is a useful technique for the characterization of metal NPs in solution [24–27]. We have previously shown that both Fe metal oxidation and galvanic redox reactions of $Fe@Fe_xO_y$ particles with Pd(II) and Cu(II) can be followed by *in situ* XANES [17,28]. Coordination environment changes can also be followed; for example, recently we monitored the reaction of Pd(II) acetate with $Au_{25}(SC_8H_9)_{18}^-$ clusters, and found that Pd(II) acetate was converted to Pd(II) thiolate species through the reaction with S atoms in the staple motifs (-S-Au-S-Au-S-) of the $Au_{25}(SC_8H_9)_{18}^-$ clusters as determined from the changes in the XANES spectra [29]. Based on the results of *in situ* Au L_3-edge XANES spectra on supported-partially oxidized Au NPs, Haider et al. proposed that metallic Au is the active species in the aerobic liquid-phase oxidation of alcohols. The conversion of 1-phenylethanol in the oxidation reaction increased with the concomitant reduction of Au species and did not decrease even after the disappearance of oxidized Au species [30].

Herein, we have synthesized $Fe@Fe_xO_y/Pd$ NPs with different molar ratios of Fe to Pd (50:1, 20:1 and 5:1) through galvanic exchange reactions. We also applied the resulting $Fe@Fe_xO_y/Pd$ NPs for the hydrogenation of 2-methyl-3-buten-2-ol in a solution of either water or ethanol, and showed they could be magnetically recovered and/or agitated during the reaction. Additionally, we carried out *in situ* XANES experiments to study catalytic speciation in different solvents during the hydrogenation reaction, to better understand differences in catalytic behavior in the different solvents. The magnetic response of 50:1 and 20:1 $Fe@Fe_xO_y/Pd$ NPs shows that they hold promise for the design of real nanometer-sized magnetic stir bars for microscopic reactions. The results of the studies indicated that $Fe@Fe_xO_y/Pd$ NPs have a higher catalytic activity in ethanol compared to water for hydrogenation reactions, and *in situ* XANES experiments reveal that these NPs are more stable in ethanol solution, whereas further oxidation of the Fe cores occurs in the presence of water.

2. Experimental section

2.1. Materials

All chemicals were used as received without further purification. Iron (II) sulfate heptahydrate, methylene blue and

Please cite this article in press as: Y. Yao, et al., In situ X-ray absorption spectroscopic studies of magnetic $Fe@Fe_xO_y/Pd$ nanoparticle catalysts for hydrogenation reactions, Catal. Today (2017), http://dx.doi.org/10.1016/j.cattod.2017.02.049

2-methyl-2-butanol were purchased from Sigma-Aldrich. Poly(vinylpyrrolidone) (M.W. 58,000 g/mol), 2-methyl-3-buten-2-ol and palladium (II) nitrate hydrate were purchased from Alfa Aesar. Sodium borohydride, ethanol and methanol (HPLC grade) were purchased from Fisher Scientific. Sulfuric acid was purchased from EMD Millipore. Eighteen MΩ·cm Milli-Q water (Millipore, Bedford, MA) was used for all syntheses.

2.2. Synthesis of Fe@Fe$_x$O$_y$/Pd NPs

Fe@Fe$_x$O$_y$ NPs were synthesized by reducing $FeSO_4 \cdot 7H_2O$ (5.0 mmol) by $NaBH_4$ (25 mmol) in a 1:1 water/methanol (v/v) mixture (20 mL) in the presence of PVP (10 mmol based on monomer unit) under nitrogen gas as previously reported [28]. First a 100 mL round bottom flask with $FeSO_4 \cdot 7H_2O$ solution (8 mL in water) was purged by nitrogen gas, then PVP solution (10 mL in methanol) was added to the flask and the mixture was stirred for 10 min. Finally, a solution of $NaBH_4$ (2 mL in water) was added dropwise. After 30 min stirring, 5.0 mL of 1 M H_2SO_4 was added to remove any excess $NaBH_4$ before injecting a Pd(II) nitrate solution (20 mM) to react with the Fe@Fe$_x$O$_y$ NPs by galvanic exchange reactions, following our previous method [17].

2.3. Hydrogenation of methylene blue

A solution of $NaBH_4$ with Fe@Fe$_x$O$_y$/Pd NPs was prepared by dispersing 0.50 mL of the above solution of Fe@Fe$_x$O$_y$/Pd NPs and 0.038 g sodium borohydride in 10 mL water. A 25 μL aliquot of this mixture was injected into a 25 μL methylene blue solution (0.050 mM), which was dropped onto a hydrophobic Teflon plate located on top of a magnetic stirrer.

2.4. Hydrogenation of 2-methyl-3-buten-2-ol

A solution of 0.010 mmol Fe@Fe$_x$O$_y$/Pd NPs (molar concentration determined based on Pd content) in 5.0 mL water was added to a round bottom flask filled with 1.1 atm hydrogen gas. To this solution, a 0.20 mL 2-methyl-3-buten-2-ol (1.9 mmol) solution was added to obtain a 190:1 substrate to catalyst molar ratio. The pressure was monitored by a differential pressure manometer (407910, Extech Instrument), and the reaction progress was also followed by ^{1}H NMR by extracting products from the reaction solutions with 2 mL aliquots of $CDCl_3$. Turnover frequencies (TOFs) were measured by plotting either product conversion or H_2 consumption (as a proxy for product conversion, a direct correspondence between NMR results and H_2 pressure decay was always observed) over reaction time. These results are reported in either (moles product formed/moles Pd)/time or (moles H_2 consumed/moles Pd)/time.

2.5. Characterization

Transmission electron microscopy (TEM) analyses of the NPs were initially conducted using a HT7700 microscope (Hitachi High-Technologies) operating at 100 kV. The samples were prepared by drop-casting one drop of dilute, aqueous sample onto a carbon-coated 200 mesh copper grid (Electron Microscopy Sciences, Hatfield, PA).

Elemental maps were obtained using an FEI Osiris STEM equipped with ChemiSTEM Technology integrating the signal from four Energy Dispersive X-ray (EDX) spectrometers. A 200 kV electron beam was focused to a nanometer-sized spot and scanned across the sample to excite electrons from the core shells. As the electron beam is raster scanned across the sample, a full X-ray spectrum is collected for each pixel. By selecting the appropriate energy window, a specific element is selected and its distribution in the sample can be displayed as an elemental map. By selecting several windows, different elemental maps can be obtained simultaneously from a single scan, provided that the ionization energies do not significantly overlap. False color maps can be also superimposed to determine where two or more elements coexist and in what relative amounts. Scanning time and beam intensity were chosen as a compromise between signal-to-noise ratio and radiation damage to the sample.

Fe K-edge and Pd L-edge XANES spectra were collected at the Soft X-ray Microcharacterization Beamline (SXRMB) at the Canadian Light Source (CLS). The measurements were conducted under an ambient atmosphere for observing the Fe K-edge and under helium for obtaining the Pd L$_3$-edge spectra. Decreasing the beam flux by defocusing and/or filtering the beam with Kapton filters and stirring the sample *via* magnetic stirring were used to avoid sample damage due to photoreduction. Liquid cells (SPEX CertiPrep Disposable XRF X-Cell sample cups) were covered with a 4 μm ultralene film (purchased from Fisher Scientific, Ottawa, ON) and used for XANES analysis. The data were analyzed using the IFEFFIT software package [31,32].

The ^{1}H NMR spectra were recorded in $CDCl_3$ on a Bruker 500 MHz Advance NMR spectrometer. Chemical shifts were recorded in parts per million (ppm), using the residual solvent peak for calibration. The composition of the reaction mixture was analyzed by a gas chromatography (GC, Agilent Technologies 7890A) with a flame ionization detector and a HP-5 capillary column (30 m × 0.32 mm × 0.25 μm, J&W Scientific).

3. Results and discussions

3.1. Synthesis and STEM analysis of Fe@Fe$_x$O$_y$/Pd NPs

The Fe@Fe$_x$O$_y$ NPs (16.0 ± 6.0 nm) were synthesized by reducing $FeSO_4 \cdot 7H_2O$ with $NaBH_4$ in a mixture of ethanol and water (1:1 volume ratio) containing PVP as a stabilizer [28]. Different molar ratios of Fe@Fe$_x$O$_y$/Pd (prepared as 50:1, 20:1, and 5:1 based on Fe:Pd molar ratios) NPs were synthesized by mixing the solution of Fe@Fe$_x$O$_y$ NPs with a Pd(II) nitrate solution under nitrogen gas purging as described previously [17]. Fig. 1A and C shows dark field STEM images of the particles synthesized at the 20:1 and 5:1 Fe:Pd molar ratios, respectively. The Fe@Fe$_x$O$_y$ particles self-assemble into larger chain-like nanostructures, presumably due to magnetic interactions between particles in solution (Fig. S1) [28]. As shown in the STEM elemental maps (Fig. 1B), the 20:1 Fe@Fe$_x$O$_y$/Pd NPs have isolated small Pd NPs (3 ± 2 nm) deposited on the surfaces of the Fe@Fe$_x$O$_y$ NPs. In the system of 5:1 Fe@Fe$_x$O$_y$/Pd NPs most of the Fe@Fe$_x$O$_y$ NPs have been consumed in the galvanic exchange formation, leaving a hybrid material that contains a fairly well-dispersed Pd on the surfaces of these Fe oxidation supports (Fig. 1D). It was very difficult to resolve individual Pd NPs in the samples containing a higher Pd loading. These results agree with previous EXAFS results on Fe@Fe$_x$O$_y$/Pd NPs from our group; the lowest first shell Pd coordination numbers, and thus highest dispersions, were seen for 5:1 Fe:Pd ratios [17].

3.2. Magnetic recovery/agitation with Fe@Fe$_x$O$_y$/Pd NPs

Fe supported bimetallic NPs have been applied in a variety of catalytic reactions [13–16,33,34]. The presence of Fe in these bimetallic NPs not only allows them to be easily separated from reaction solutions by an external magnet, but can also act as a redox scavenger to redeposit the leached metal and avoid the contamination of the organic product. Fe atoms have a strong magnetic moment due to their high number of unpaired 3d electrons, thus Fe and Fe oxide materials exhibit strong magnetic properties [35].

Please cite this article in press as: Y. Yao, et al., In situ X-ray absorption spectroscopic studies of magnetic Fe@Fe$_x$O$_y$/Pd nanoparticle catalysts for hydrogenation reactions, Catal. Today (2017), http://dx.doi.org/10.1016/j.cattod.2017.02.049

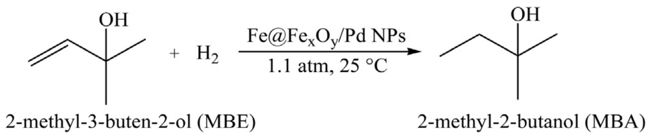

Scheme 1. The hydrogenation of 2-methyl-3-buten-2-ol.

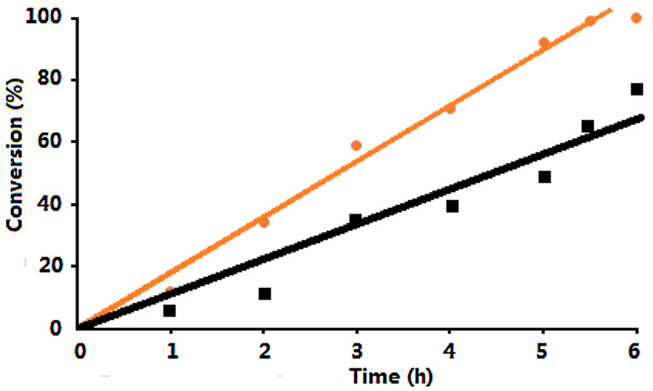

Fig. 2. The conversion of 2-methyl-3-buten-2-ol to 2-methyl-2-butanol in the hydrogenation reaction (black square) using the 50:1 $Fe@Fe_xO_y/Pd$ NPs as catalysts without stirring, and (orange dot) using 50:1 $Fe@Fe_xO_y/Pd$ NPs as both catalysts and magnetic stirrers in a 5 mL solution. (For interpretation of the references to color in this figure legend, the reader is referred to the web version of this article.)

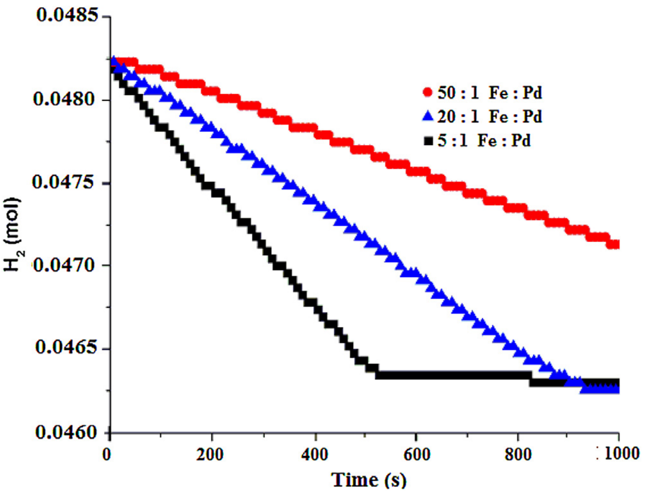

Fig. 3. The rate of hydrogen consumption in the hydrogenation of 2-methyl-3-buten-2-ol in water using the 50:1 (red circle), 20:1 (blue triangle) and 5:1 (black square) $Fe@Fe_xO_y/Pd$ NPs as catalysts. (For interpretation of the references to color in this figure legend, the reader is referred to the web version of this article.)

The large surface area to volume ratio of Fe and Fe oxide NPs can result in increased remanence and coercivity and can give these NPs improved magnetic properties in comparison to their bulk counterparts [36,37]. The fact that the original $Fe@Fe_xO_y$ NPs self-assemble into larger domains may allow them to be used for stirring at the microscopic scale. Indeed this is the case for the $Fe@Fe_xO_y/Pd$ NPs synthesized with 50:1 and 20:1 molar ratios of $Fe@Fe_xO_y$ NPs to Pd(II). The resulting NPs have strong responses to the magnetic field of a common stir plate, and allow for a solution to be stirred in the absence of a macroscopic stir bar (Fig. S2). However, the $Fe@Fe_xO_y/Pd$ NPs synthesized with a 5:1 molar ratio of $Fe@Fe_xO_y$ NPs to Pd(II) do not agitate a solution upon magnetic stirring. In addition, we examined the relative ease of magnetically separating each of the NP systems from solution. The 50:1 and 20:1 $Fe@Fe_xO_y/Pd$ NPs could be separated by an external magnet from the reaction solutions after 9 s (Fig. S3), while the separation of the 5:1 $Fe@Fe_xO_y/Pd$ NPs from solution takes a much longer time (more than 30 s). These results indicate the possibility of using these bimetallic catalysts as magnetically recoverable catalysts and magnetic stirrers, provided that the Pd loading is not too high.

To further test whether $Fe@Fe_xO_y/Pd$ NPs can improve the reaction rate for catalytic reactions by alleviating mass transfer issues, we applied the $Fe@Fe_xO_y/Pd$ NPs as catalysts and microscopic stirrers for the hydrogenation of 2-methyl-3-buten-2-ol in water under a 1.1 atm H_2 gas at 25 °C (Scheme 1). The addition of the 50:1 $Fe@Fe_xO_y/Pd$ NPs as catalysts yielded a TOF of 21 h^{-1} for the hydrogenation of 2-methyl-3-buten-2-ol to 2-methyl-2-butanol as determined by NMR in the absence of stirring, whereas the TOF was improved to 34 h^{-1} by stirring the solution using the 50:1 $Fe@Fe_xO_y/Pd$ NPs (Fig. 2). This result confirms that the NPs can improve mass-transfer of the substrates to the catalyst surface. As the temperature of the reaction flask was kept constant at 25 °C, we do not believe that magnetic heating was a factor. As this test was performed on a 5 mL sample and not a droplet with a small volume, the difference between the stirred and non-stirred states is not significant. A microscopic model test system was also carried out using $Fe@Fe_xO_y/Pd$ NPs to catalyze the hydrogenation of methylene blue (MB) within small liquid droplets. Solutions containing either 50:1 or 20:1 $Fe@Fe_xO_y/Pd$ NPs and $NaBH_4$ were injected into the MB droplet. MB could be reduced by the $NaBH_4$ and converted to a colorless leucomethylene blue solution in 30 s when agitated by the 50:1 or 20:1 $Fe@Fe_xO_y/Pd$ NPs (Fig. S4). In comparison, it was difficult to reduce MB by the addition of $NaBH_4$ without the stirring of NPs. This study reveals that the agitation of the 50:1 and 20:1 $Fe@Fe_xO_y/Pd$ NPs using an external magnetic field can effectively mix the reactants and improve the reaction rate.

3.3. Catalytic behavior in the hydrogenation of 2-methyl-3-buten-2-ol

Having established that the $Fe@Fe_xO_y/Pd$ NPs can be effective catalysts, we sought to optimize the catalyst system in terms of the Pd loading, solvent composition, and long-term stability of the catalyst. For these studies larger volumes of solutions were used along with a macroscopic magnetic stir bar (egg shaped, 7/8 in. × 3/8 in.) rotated at 1600 rpm. Fig. S5 shows that the rotation with a macroscopic magnetic stir bar can speed up the reaction rate much more at higher temperatures compared to the reaction rates at the same temperatures without any stirring (Fig. S6), which shows that stirring can minimize mass transfer effects for the hydrogenation reactions and thus allow a better comparison of actual catalytic activities. The progress of the reaction was monitored by measuring the decrease in pressure of H_2 filled in a round bottom flask as a function of reaction time. When $Fe@Fe_xO_y$ NPs (in the absence of Pd) were used as the catalyst for the hydrogenation of 2-methyl-3-buten-2-ol in water at 1.1 atm H_2 (g) and 25 °C, there was no decrease in the pressure of H_2. However, $Fe@Fe_xO_y/Pd$ NP catalysts (50:1, 20:1 and 5:1 Fe:Pd molar ratios) exhibit high TOFs. As shown in Fig. 3, the reaction follows a zero order rate law, and reaches completion once all the substrate is consumed. The decrease of the moles of the H_2 gas in the reaction from 0.0482 mol to 0.0463 mol reveals that the consumption of H_2 is 1:1 with respect to the substrate 2-methyl-3-buten-2-ol (1.9 mmol used for the reaction). The 5:1 $Fe@Fe_xO_y/Pd$ NPs showed the highest TOF (*ca.* 1300 h^{-1}) in comparison to the 50:1 and 20:1 $Fe@Fe_xO_y/Pd$ NPs (TOF of 385 h^{-1} and 785 h^{-1}, respectively). As noted earlier, $Fe@Fe_xO_y$ NP controls showed no activity for hydrogenations, confirming that Pd is the active catalyst for this reaction. The higher TOF of 5:1 $Fe@Fe_xO_y/Pd$ NPs compared to 50:1 and 20:1 $Fe@Fe_xO_y/Pd$ NPs suggests that the Pd is more dispersed and has a higher surface area for the

Please cite this article in press as: Y. Yao, et al., In situ X-ray absorption spectroscopic studies of magnetic $Fe@Fe_xO_y/Pd$ nanoparticle catalysts for hydrogenation reactions, Catal. Today (2017), http://dx.doi.org/10.1016/j.cattod.2017.02.049

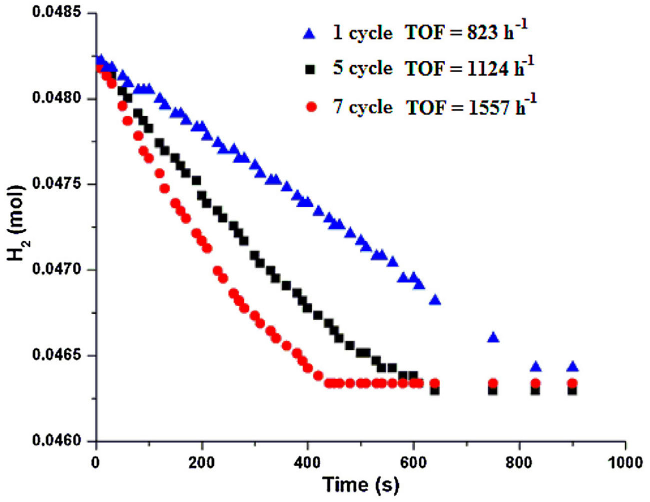

Fig. 4. The rates of hydrogen consumption in the hydrogenation of 2-methyl-3-buten-2-ol in water using the 20:1 $Fe@Fe_xO_y/Pd$ NPs recycled for the use in sequential catalytic cycles.

5:1 $Fe@Fe_xO_y/Pd$ NPs, which is in agreement with the results of elemental EDX maps shown earlier.

The reusability of the $Fe@Fe_xO_y/Pd$ NPs was also examined by using 20:1 $Fe@Fe_xO_y/Pd$ NPs as an example. These NPs were recycled by isolating the NPs from solution using centrifugation. The results of this evaluation are summarized in Fig. 4. Surprisingly, the $Fe@Fe_xO_y/Pd$ NPs exhibited a higher catalytic activity upon recycling. However, it also became successively more difficult to fully recover the material with an external magnet. The TEM images show that there are fewer and/or significantly smaller $Fe@Fe_xO_y$ NPs remaining in the bimetallic NPs system as the number of cycles increased (Fig. 5). The result suggests that the $Fe@Fe_xO_y$ NPs are degrading over time. This conclusion is also supported by *ex situ* XANES measurements, as shown in Fig. 6. There is almost no change in the speciation of the zerovalent Pd NPs as judged by comparing the Pd L_3-edge XANES spectra after different recycling tests (Fig. 6A), while the Fe K-edge XANES spectra show a significant shift to higher energies upon using the catalysts over 6 cycles (Fig. 6B). These results are consistent with the progressive oxidation of the $Fe@Fe_xO_y$ NPs to Fe(II) and Fe(III) oxides [28].

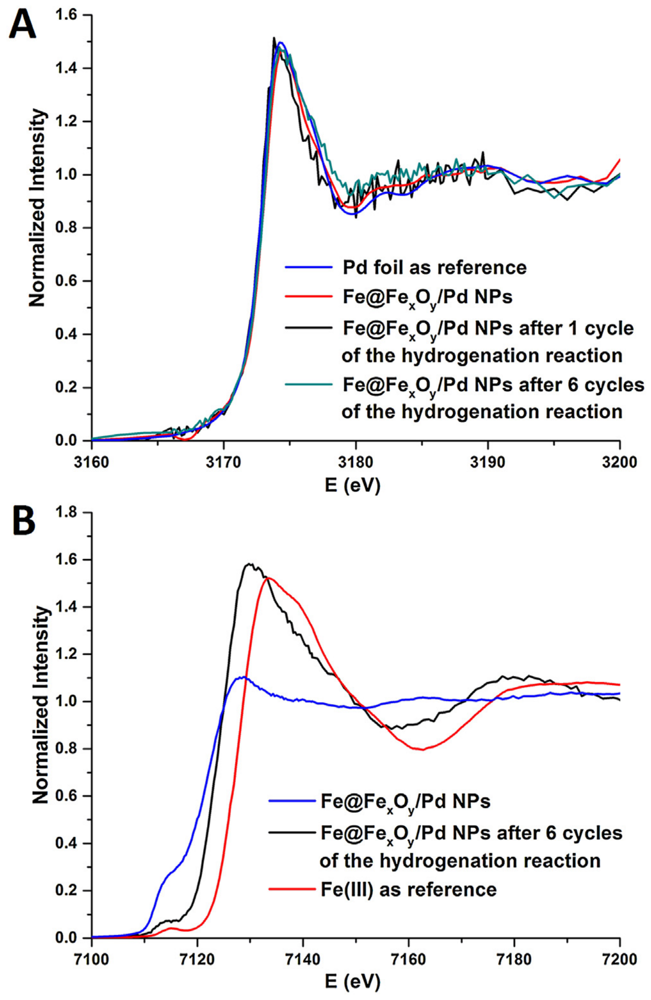

Fig. 6. The Pd L-edge (A) and Fe K-edge (B) XANES spectra of the 20:1 molar ratio $Fe@Fe_xO_y/Pd$ NPs.

To determine whether the oxidation of $Fe@Fe_xO_y$ NPs takes place during the hydrogenation reaction or during the recycling process, *in situ* XANES studies were carried out. The *in situ* setup is shown in Fig. 7, and consisted of a liquid cell loaded with $Fe@Fe_xO_y$ NPs and 2-methyl-3-buten-2-ol in water, and placed inside an aluminum box which was located on top of a magnetic stirrer (not shown) to ensure the constant mixing of the reaction mixture. Hydrogen gas was bubbled into the liquid cell to start the reaction and the reaction was monitored at the Pd L_3 and Fe K edges, as shown in Fig. 8. No significant change of the *in situ* Pd L_3-edge XANES spectra was observed (Fig. 8A), which is not overly surprising as Pd typically remains in the zerovalent state during hydrogenation reactions [38]. However, slight oxidation of the $Fe@Fe_xO_y$ NPs could be observed from *in situ* Fe K-edge XANES spectra (Fig. 8B). Through fitting the Fe K-edge XANES spectra using a linear combination fitting with standards (Fe foil, $FeSO_4$ and $Fe(NO_3)_3$) as we did in our previous work [28], it is revealed that the $Fe@Fe_xO_y$ NPs in the $Fe@Fe_xO_y/Pd$ NP systems contain 56% Fe(0) (Table S1). These standards were chosen as they led to the best fits of the experimental data; we were not able to fit the data

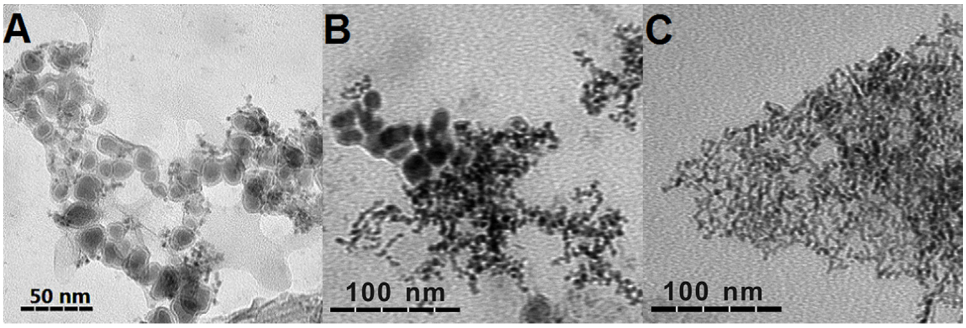

Fig. 5. TEM images of the 20:1 $Fe@Fe_xO_y/Pd$ NPs: (A) before hydrogenation reaction; (B) after 4 cycles; and (C) after 6 cycles.

Please cite this article in press as: Y. Yao, et al., In situ X-ray absorption spectroscopic studies of magnetic $Fe@Fe_xO_y/Pd$ nanoparticle catalysts for hydrogenation reactions, Catal. Today (2017), http://dx.doi.org/10.1016/j.cattod.2017.02.049

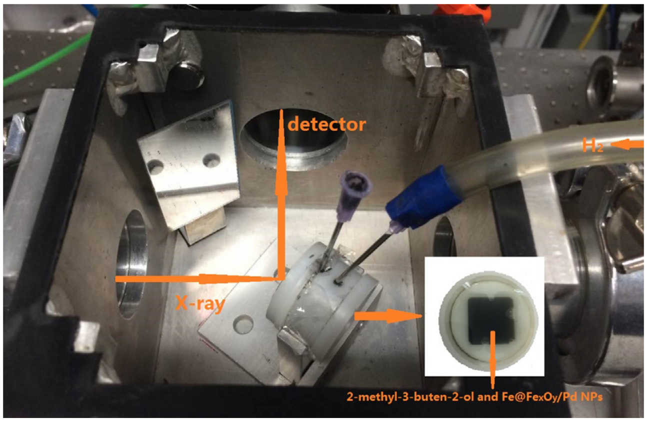

Fig. 7. The hydrogenation setup for *in situ* fluorescence XANES studies.

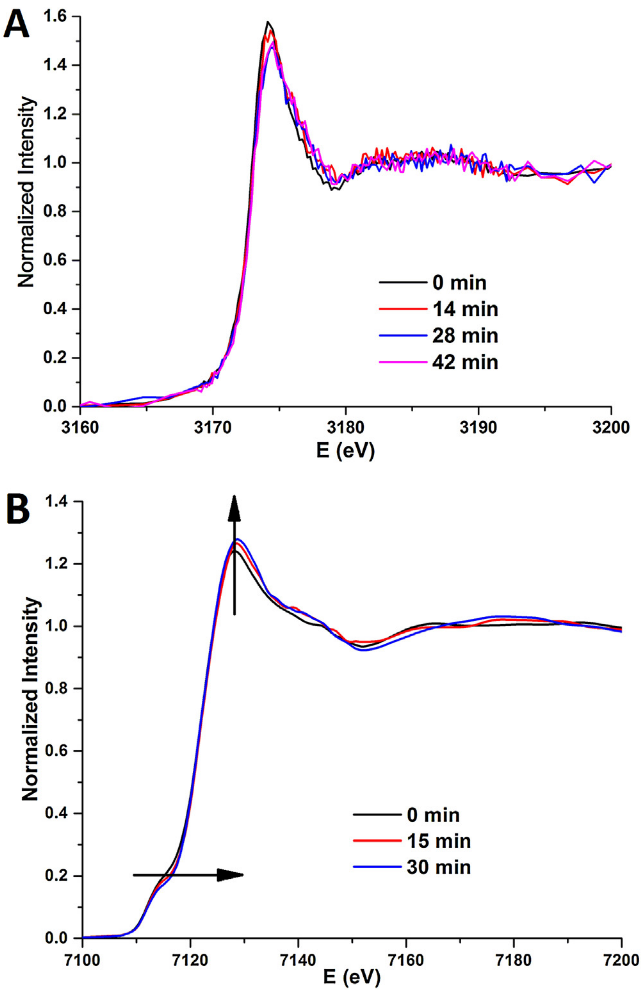

Fig. 8. The Pd L-edge (A) and Fe K-edge (B) XANES spectra of the 20:1 molar ratio $Fe@Fe_xO_y/Pd$ NPs in the hydrogenation reaction using water as a solvent.

using standards involving different oxide and hydroxide phases of Fe. This Fe(0) content decreases to 49% after 30 min of the hydrogenation reaction in water, and all the Fe(0) was oxidized after 6 cycles (to 60% Fe(II) and 40% Fe(III), the fitted data from Fig. 6B, Table S2). This result indicates that the oxidation of $Fe@Fe_xO_y$ NPs happens during the reaction. We note that water is the solvent for this reaction; water can react with exposed Fe in $Fe@Fe_xO_y$ NPs and oxidize Fe(0) to Fe(II), which is likely the reason for oxidation of the $Fe@Fe_xO_y$ NPs in the reaction [39]. The Fe(II) is then further oxidized to Fe(III) during the recycling process when the samples are exposed to air.

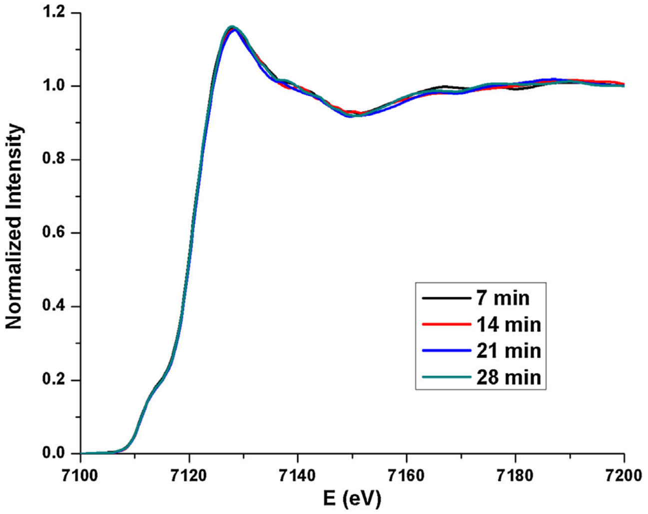

Fig. 9. The Fe K-edge XANES spectra of the 20:1 $Fe@Fe_xO_y/Pd$ NPs in the hydrogenation reaction using ethanol as a solvent.

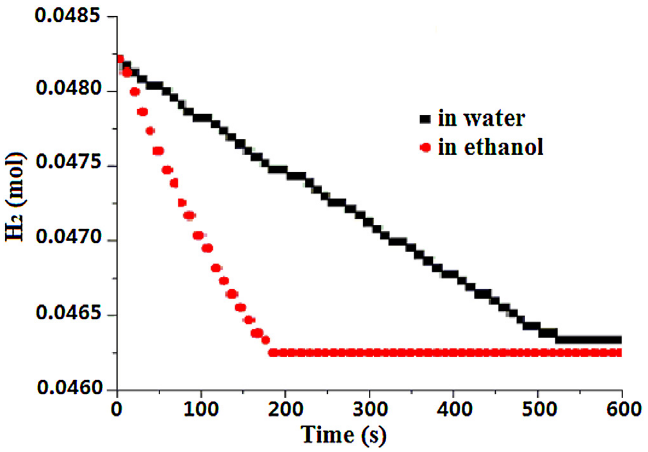

Fig. 10. The rates of hydrogen consumption for the hydrogenation of 2-methyl-3-buten-2-ol using the 5:1 $Fe@Fe_xO_y/Pd$ NPs as catalysts in either water or ethanol.

In order to address this oxidation damage to the NPs, we switched the solvent from water to ethanol for the hydrogenation reactions, as ethanol should not react with Fe(0). The Pd L_3-edge XANES spectra indicate that the Pd NPs have no change before and after the hydrogenation reaction in ethanol (Fig. S7). There is also no change observed in the *in situ* Fe K-edge XANES spectra (Fig. 9). These results confirm that the $Fe@Fe_xO_y$ NPs are quite stable in ethanol. The $Fe@Fe_xO_y/Pd$ NPs also showed a much higher catalytic activity in ethanol than in water, as shown in Fig. 10. The 5:1 $Fe@Fe_xO_y/Pd$ NPs showed improvements in TOF from *ca.* 1300 h^{-1} in water to 3600 h^{-1} in ethanol, an increase of 2.8 times in magnitude. The NMR and GC results confirmed that the conversion of 2-methyl-3-buten-2-ol to 2-methylbutan-2-ol is completed in 4 min when catalyzed by 5:1 $Fe@Fe_xO_y/Pd$ NPs with a 190:1 substrate to catalyst ratio in ethanol. No change was seen in the TOF for the hydrogenation reaction upon recycling the catalysts for three cycles in ethanol, and no significant changes were seen by TEM (Fig. S8). This catalytic result is a very high TOF for the hydrogenation of 2-methyl-3-buten-2-ol under ambient conditions, and compares favourably with many excellent hydrogenation catalysts in the literature [40–43]. The factors determining solvent influence in the hydrogenation reactions have

Please cite this article in press as: Y. Yao, et al., In situ X-ray absorption spectroscopic studies of magnetic $Fe@Fe_xO_y/Pd$ nanoparticle catalysts for hydrogenation reactions, Catal. Today (2017), http://dx.doi.org/10.1016/j.cattod.2017.02.049

been studied by many groups [38,44–48]. The solubility of H_2 (g) seems to be the most significant factor influencing the rate of this reaction along with the high stability of the support in ethanol. The solubility of H_2 (2.98×10^{-3} mol/L) in ethanol is significantly higher than that in water (0.81×10^{-3} mol/L) [49]. These results are also consistent with Nikoshvili group's studies on the selective and solvent dependent hydrogenation of 2-methyl-3-butyn-2-ol to 2-methyl-3-buten-2-ol over Pd NPs stabilized in hypercrosslinked polystyrene [38].

4. Conclusion

A suspension of either 50:1 or 20:1 $Fe@Fe_xO_y/Pd$ NPs can act as both magnetically recoverable catalysts and magnetic stirrers to improve the mixing of reactants in catalytic hydrogenation reactions. For studies on the catalytic activity of the $Fe@Fe_xO_y/Pd$ NPs for the hydrogenation of 2-methyl-3-buten-2-ol, the 5:1 molar ratio $Fe@Fe_xO_y/Pd$ NPs exhibit a high TOF of 3600 h^{-1} using ethanol as the solvent. *In situ* XANES spectra show that water as a solvent in the hydrogenation reaction can oxidize the Fe(0) core in $Fe@Fe_xO_y/Pd$ NPs, while the same $Fe@Fe_xO_y/Pd$ NPs are very stable when dispersed in ethanol. This result shows that while these composite materials have viability as low cost, magnetically recoverable catalysts, they do not have long-term stability in water which may limit their possible applications.

Acknowledgements

The authors thank William Barrett for assistance with hydrogenation reactions. The authors acknowledge financial assistance from the National Sciences and Engineering Research Council of Canada "(NSERC Discovery Grant No. 1077758) and the Canada Research Chairs Program (B.D. Gates, Grant No. 950-215846). XANES experiments described in this paper were performed at the Canadian Light Source, which is supported by NSERC, the National Research Council Canada, the Canadian Institutes of Health Research, the Province of Saskatchewan, Western Economic Diversification Canada, and the University of Saskatchewan. This work also made use of 4D LABS (www.4dlabs.ca) shared facilities supported by the Canada Foundation for Innovation (CFI), British Columbia Knowledge Development Fund (BCKDF), Western Economic Diversification Canada, and Simon Fraser University.

References

[1] M. Haruta, T. Kobayashi, H. Sano, N. Yamada, Chem. Lett. 2 (1987) 405–408.
[2] R.V. Jagadeesh, A. Surkus, H. Junge, M. Pohl, J. Radnik, H. Huan, V. Schünemann, A. Brückner, M. Beller, Science 342 (2013) 1073–1076.
[3] H. Zhang, M. Jin, Y. Xia, Chem. S oc. Rev. 41 (2012) 8035–8049.
[4] T. Sun, Y. Zhang, B. Pang, D.C. Hyun, M. Yang, Y. Xia, Angew. Chem. Int. Ed. 53 (2014) 12320–12364.
[5] A. Kaur, U.J. Gupta, Mater. Chem. 19 (2009) 8279–8289.
[6] R. Sachan, A. Malasi, J. Ge, S. Yadavali, H. Krishna, A. Gangopadhyay, H. Garcia, G. Duscher, R. Kalyanaraman, ACS Nano 8 (2014) 9790–9798.
[7] A. Schejn, T. Mazet, V. Falk, L. Balan, L. Aranda, G. Medjahdi, R. Schneider, Dalton Trans. 44 (2015) 10136–10140.
[8] R. Hudson, Y. Feng, R.S. Varma, A. Moores, Green Chem. 16 (2014) 4493–4505.
[9] A.Y. Li, M. Kaushik, C.-J. Li, A. Moores, ACS Sustainable Chem. Eng. 4 (2016) 965–973.
[10] W.H. Chong, L.K. Chin, R.L.S. Tan, A.Q. H.Wang, H. Liu, Angew. Chem. Int. Ed. 52 (2013) 8570–8573.
[11] S. Yang, C. Cao, Y. Sun, P. Huang, F. Wei, W. Song, Angew. Chem. Int. Ed. 54 (2015) 2661–2664.
[12] CRC Handbook of Chemistry and Physics, 96th ed., CRC Press, Cleveland, OH, 2010.
[13] S. Zhou, M. Johnson, J.G.C. Veinot, Chem. Commun. 46 (2010) 2411–2413.
[14] R. Hudson, C.J. Li, A. Moores, Green Chem. 14 (2012) 622–624.
[15] R. Hudson, V. Chazelle, M. Bateman, R. Roy, C.J. Li, A. Moores, A.C.S. Sustain, Chem. Eng. 3 (2015) 814–820.
[16] Y. Zhang, Y. Su, X. Zhou, C. Dai, A.A. Keller, J. Hazard Mater. 263 (2013) 685–693.
[17] Y. Yao, C. Patzig, Y. Hu, R.W.J. Scott, J. Phys. Chem. C 119 (2015) 21209–21218.
[18] S. Ishikawa, R. Hudson, M. Masnadi, M. Bateman, A. Castonguay, A. Moores, C.J. Li, Tetrahedron 70 (2014) 6162–6168.
[19] S. Nishimura, Handbook of Heterogeneous Catalytic Hydrogenation for Organic Synthesis, John Wiley & Sons, New York, 2001.
[20] P.N. Rylander, Hydrogenation Methods, Academic Press, New York, 1985.
[21] H. Sajiki, T. Ikaea, K. Hirota, Tetrahedron Lett. 42 (2001) 7699–7701.
[22] T. He, L. Liu, G. Wu, P. Chen, J. Mater. Chem. A 3 (2015) 16235–16241.
[23] J. Yuan, Pesticides 46 (2007) 827–829.
[24] R.M. Anderson, L. Zhang, J.A. Loussaert, A.I. Frenkel, G. Henkelman, R.M. Crooks, ACS Nano 10 (2013) 9345–9353.
[25] L. Wang, S. Zhang, Y. Zhu, A. Patlolla, J. Shan, H. Yoshida, S. Takeda, A.I. Frenkel, F. Tao, ACS Catal. 3 (2013) 1011–1019.
[26] J. Ohyama, K. Teramura, T. Shishido, Y. Hitomi, K. Kato, H. Tanida, T. Uruga, T. Tanaka, Chem. Phys. Lett. 507 (2011) 105–110.
[27] A. Maclennan, A. Banerjee, Y. Hu, J.T. Miller, R.W.J. Scott, ACS Catal. 3 (2013) 1411–1419.
[28] Y. Yao, Y. Hu, R.W.J. Scott, J. Phys. Chem. C 118 (2014) 22317–22324.
[29] A. Shivhare, K.E. Lee, Y. Hu, R.W.J. Scott, J. Phys. Chem. C 119 (2015) 23279–23284.
[30] P. Haider, J.D. Grunwaldt, R. Seidel, A. Baiker, J. Catal. 250 (2007) 313–323.
[31] M. Newville, J. Synchrotron Radiat. 8 (2001) 322–324.
[32] B. Ravel, M. Newville, J. Synchrotron Radiat. 12 (2005) 537–541.
[33] S. Kovács, K. Zih-Perényi, Á. Révész, Z. Novák, Synthesis 44 (2012) 3722–3730.
[34] S. Kovács, Z. Novák, Org. Biomol. Chem. 9 (2011) 711–716.
[35] P. Wasilewski, G. Kletetschka, Geophys. Res. Lett. 26 (1999) 2275–2278.
[36] B. Issa, I.M. Obaidat, B.A. Albiss, Y. Haik, Int. J. Mol. Sci. 14 (2013) 21266–21305.
[37] D.K. Kim, Y. Zhang, W. Voit, K.V. Rao, M. Muhammed, J. Magn. Magn. Mater. 225 (2001) 30–36.
[38] L. Nikoshvili, E. Shimanskaya, A. Bykov, I. Yuranov, L. Kiwi-Minsker, E. Sulman, Catal. Today 241 (2015) 179–188.
[39] X. Li, D.W. Elliott, W. Zhang, Rev. Crit. Env. Sci. Technol. 31 (2006) 111–122.
[40] R. Ma, N. Semagina, J. Phys. Chem. C 114 (2010) 15417–15423.
[41] J. Shen, N. Semagina, ACS Catal. 4 (2014) 268–279.
[42] A. Banerjee, R.W.J. Scott, Green Chem. 17 (2015) 1597–1604.
[43] Y. Niu, L.K. Yeung, R.M. Crooks, J. Am. Chem. Soc. 123 (2001) 6840–6846.
[44] E. Sadeghmoghaddam, H. Gu, Y.S. Shon, ACS Catal. 2 (2012) 1838–1845.
[45] N.M. Bertero, A.F. Trasarti, C.R. Apesteguia, A. Marchi, J. Appl. Catal. A: Gen. 394 (2011) 228–238.
[46] R.A. Rajadhyskasha, S.I. Karwa, Chem. Eng. Sci. 41 (1986) 1765–1770.
[47] R.L. Augustine, R.W. Warner, M.J. Melnick, J. Org. Chem. 49 (1984) 4853–4856.
[48] E. Toukoniitty, P. Mäki-Arvela, J. Kuusisto, V. Nieminen, J. Päivärinta, M. Hotokka, T. Salmi, D. Yu Murzin, J. Mol. Catal. 192 (2002) 135–151.
[49] M. Ghavre, S. Morrissey, N. Gathergood, Hydrogenation in ionic liquids, Ionic Liq. Appl. Perspect. (2011) 331–392.

Please cite this article in press as: Y. Yao, et al., In situ X-ray absorption spectroscopic studies of magnetic $Fe@Fe_xO_y/Pd$ nanoparticle catalysts for hydrogenation reactions, Catal. Today (2017), http://dx.doi.org/10.1016/j.cattod.2017.02.049